JOURNAL OF SOLID STATE CHEMISTRY 113, 182–192 (1994)

Acid-Delithiated $Li_{1-x}(Ni_yCo_{1-y})_{1+x}O_2$ as Insertion Electrodes in Lithium Batteries

J. Morales,* R. Stoyanova,† J. L. Tirado,* and E. Zhecheva†

*Departamento de Química Inorgánica e Ingeniería Química, Facultad de Ciencias, Universidad de Córdoba, 14004 Córdoba, Spain; and †Institute of General and Inorganic Chemistry, Bulgarian Academy of Sciences, 1113 Sofia, Bulgaria

Received October 1, 1993; accepted February 10, 1994

Monophase $Li_{1-x}(Ni_yCo_{1-y})_{1+x}O_2$ oxides ($0 \le y \le 0.4$ and $0.8 \le y \le 0.9$) with a layered structure ($R\bar{3}m$ space group) have been prepared by interaction of $(Ni_yCo_{1-y})_3O_4$ ($0 \le y \le 0.4$) and $Ni_yCo_{1-y}O$ ($0.8 \le y \le 0.9$) with LiOH at low temperature (450°C). As in the case of high-temperature analogues, cobalt substitution for nickel stabilizes the Ni^{3+} ions and improves the two-dimensionality of the crystal lattice. Acid treatment of LT and HT oxides leads to a partial dissolution of the solid and to removal of lithium and "impurity" cobalt and/or nickel from LiO_2 layers of the trigonal framework. For cobalt-rich oxides, the ion extraction is accompanied by partial Li^+/H^+ exchange, especially for LT samples. Acid-delithiated oxides are studied as cathode materials in lithium batteries. The resulting cells show a high value of the initial voltage (4 V), which allows a direct discharge of the cell without previous charge. For LT samples, the discharge and charge processes occur at lower voltage (especially for Co-rich oxides) and the reversibility of the cell is lower as compared to that of HT analogues. The better reversibility of the cell in the 4.0–3.2 V range is found for HT Ni-rich oxide. The composition of the acid-treated oxides can be recovered without an enhancement polarization of the cell. XRD analysis and IR spectroscopy show good reversibility of lithium insertion and extraction reactions by chemical and electrochemical procedures.

INTRODUCTION

In the past decades, studies on the intercalation chemistry of inorganic solids have proliferated on account of their technological significance in various fields. Particularly, the optimization of intercalation positive electrodes in lithium batteries has been the subject of extensive research, as lithium batteries offer interesting advantages due to the low weights and high energy densities obtained. At present, several oxide systems allow adequate battery performances. These include several manganese, nickel, and cobalt compounds, which have been extensively investigated in the past years. From these systems, several prototypes and commercial products have recently emerged. Nagaura and Tazawa (Sony Energytec) used $Li_{1-x}CoO_2$ as cathodic material in second-generation rocking-chair batteries (1). Dahn *et al.* of Simon Fraser University (British Columbia) have used $Li_{1-x}NiO_2$ cathodes (2) and Canada's Moli Energy Ltd. is developing this battery.

From a practical point of view it is more favourable to use lithium–nickel electrodes in batteries since nickel is cheaper than cobalt and, besides, the chemical potential of intercalated lithium in $Li_{1-x}NiO_2$ is lower than in $Li_{1-x}CoO_2$ (3.5–4.0 and 3.9–4.3 V, respectively), so that the oxidation of the nonaqueous electrolyte during prolonged cycling is prevented. Unfortunately, lithium–nickel oxides are usually prepared as nonstoichiometric, $Li_{1-x}Ni_{1+x}O_2$, owing to difficult oxidation of Ni^{2+} to Ni^{3+}. Although lithium can be reversibly deintercalated in electrochemical cells between 3.5 and 4.0 V, the impurity Ni^{2+} ions perturb the layered crystal structure of $LiNiO_2$ and hinder lithium transport, which result in poor performance of the electrochemical cells.

On the other hand, recent works reported the chemical deintercalation of $Li_{1-x}Ni_{1+x}O_2$ (3, 4). This process involves the partial dissolution of the solid and nickel disproportionation, which is accompanied by lithium extraction from the layered solid. The resulting product preserves the layered structure. Moreover, the average oxidation state of nickel increases significantly and the impurity nickel ions in the interlayer space occupied by lithium ions in "stoichiometric" $LiNiO_2$ are extracted.

For $LiCoO_2$, the composition domains of three distinct phases of $Li_{1-x}CoO_2$ were established in V vs x curves at 3.93, 4.07, and 4.19 V (5). *In situ* X-ray diffraction measurements show a first order phase transition involving a significant expansion of the c lattice parameter for $0.73 \le x \le 0.93$ (3.9 V). Near $x \simeq 0.5$, the order–disorder transition of lithium ions cause a lattice distortion to a monoclinic unit cell. According to recent patents, electrodes based on $LiNi_{1-y}Co_yO_2$ solid solutions exhibit a higher capacity during cycling between 3.5 and 4.0 V than in comparison of $LiNiO_2$ and $LiCoO_2$ (6).

Recently a new $LiCoO_2$ phase (called LT-$LiCoO_2$) with

0022-4596/94 $6.00

a spinel-related structure (analogous to $Li_2Ti_2O_4$) was synthesized at low temperature (7, 8). This new material has different electrochemical performance from that of layered $LiCoO_2$ (synthesized at high temperature): LT-$LiCoO_2$ can be cycled at lower voltage (3.3–3.9 V) without significant changes in the lattice parameter. The solubility of nickel in LT-$LiCoO_2$ is restricted for $0 < Ni/(Ni + Co) \leq 0.2$. In this interval, an essentially cubic-closed packed oxygen-ion lattice is obtained with a ratio of the rhombohedral unit cell parameters $c/a = 4.90$. To our knowledge, a nickel analog of LT-$LiCoO_2$ has not been reported (9).

This research work has a three-fold aim, namely, (a) to prepare and characterize new materials in the Li–Ni–Co–O system obtained at different temperatures, (b) to study the chemical deintercalation processes in these materials, and (c) to evaluate the cathodic performance of the chemically deintercalated oxides.

EXPERIMENTAL

Two sets of samples prepared at low and high temperature (450 and 850°C, respectively) were investigated. Low-temperature samples were synthesized by a solid-state reaction between LiOH and $(Co_{1-y}Ni_y)_3O_4$ for $0 \leq y \leq 0.4$ and between LiOH and $Ni_yCo_{1-y}O$ for $0.8 \leq y \leq 1.0$. Freshly co-precipitated nickel and cobalt hydroxides were mixed with $LiOH \cdot H_2O$ in atomic ratio (Ni + Co)/Li = 1.0. The mixture was heated to 450°C at 5°/min, and this temperature was maintained for 7 days. For nickel-rich compounds, the solid-state reaction proceeds in an oxygen atmosphere.

High-temperature samples are products of the solid reaction between $LiNO_3$ and nickel–cobalt oxide. Solid Li_2CO_3 was added to a 75% solution of $Ni(NO_3)_2$ and $Co(NO_3)_2$ with intensive stirring. The mixture was evaporated at 100°C to a dry residue with the phase composition $M(OH)(NO_3) \cdot H_2O$ (M = Ni, Co) and $LiNO_3$. This intimate mixture was heated at 300°C to the complete evolution of the nitrogen oxides formed during the thermal decomposition of the hydroxynitrate. The solid residue was homogenized, pelleted, and heated at 600°C for 6 hr in air, then ground again, pelleted, and heated at 850°C in air for 30 hr.

The acid delithiation of the oxides was achieved by treating 2 g of each sample at room temperature with 100 ml of 1:20 and 1:50 v/v 36% HCl for 5 and 24 hr, respectively. The duration of treatment was experimentally determined with a view to attaining at least 40–50% dissolution of the sample. The solid residues were then dried at room temperature.

The lithium content and Ni/Co ratio were determined by atomic absorption analysis, the total (Ni + Co) content was established by complexometric titration, and the mean oxidation state of the metal ions (Ni^{3+} and/or Co^{3+}) was determined by chromatometric titration.

X-ray powder diffractometry (XRD) patterns were recorded on a Siemens D500 instrument using CuK_α radiation and a graphite monochromator. A plastic film was used as a cover during the recording of the XRD patterns in order to avoid exposure of the intercalated samples to the atmosphere. Rietveld analysis of selected patterns was carried out by using the computer program developed by Wiles and Young (10). It should be noted that due to the similar atomic scattering factors of Ni and Co ions and the various oxidation states present in the solid, the Rietveld method does not allow one to distinguish between the different situations. Thus the atomic scattering factor of Ni^{3+} was used in the analysis to describe all the transition metal ions in the structure.

FTIR spectra were obtained with a Bomem MS100 instrument. DSC measurements were carried out with a Mettler DSC20 apparatus provided with a Mettler TA3000 processing unit TG data were obtained with a Cahn 2000 electrobalance. EDX analysis was carried out in a JEOL SEM microscope. Transmission electron microscopy and electron diffraction measurements were made on a JEOL 200CX instrument.

The electrochemical intercalation–deintercalation of lithium was studied in Li/$LiClO_4$(PC)/oxide test cells. The cathode consisted of 80% active material, 10% binder, and 10% graphite. The cells were prepared inside the dry box by placing a clean metal disk, two glass fiber separators soaked with the electrolyte solution, and the cathode pellet concerned into a Teflon container with two stainless-steel terminals. The electrode area was ≈0.385 cm^2. Step potential electrochemical spectroscopy was carried out at 25°C by using a multichannel microprocessor-controlled system MacPile. An initial relaxation of the cells was allowed until the condition $\Delta V/\Delta t \leq 1$ mV/hr was fulfilled. The spectra were obtained with −10 mV/hr voltage steps. The average alkali metal composition of the cathode material was calculated from the amount of electron charge transferred to the active material, on the assumption that no current flow was due to side reactions.

RESULTS AND DISCUSSION

Synthesis and Structural Characterization of LT Oxides

Mixed hydroxide compounds of general formula $Ni_yCo_{1-y}(OH)_2$ were used as precursors to obtain LT samples. Thermal decomposition of $Ni_yCo_{1-y}(OH)_2$, which proceeds between 190 and 250°C, yields the mixed oxides with $(Ni_yCo_{1-y})_3O_4$ composition for $0 \leq y \leq 0.4$ and $Ni_yCo_{1-y}O$ composition for $0.8 \leq y \leq 1.0$ values. The interaction of $(Ni_yCo_{1-y})_3O_4$ and $Ni_yCo_{1-y}O$ with LiOH at 450°C lead to the formation of lithium–nickel–cobalt

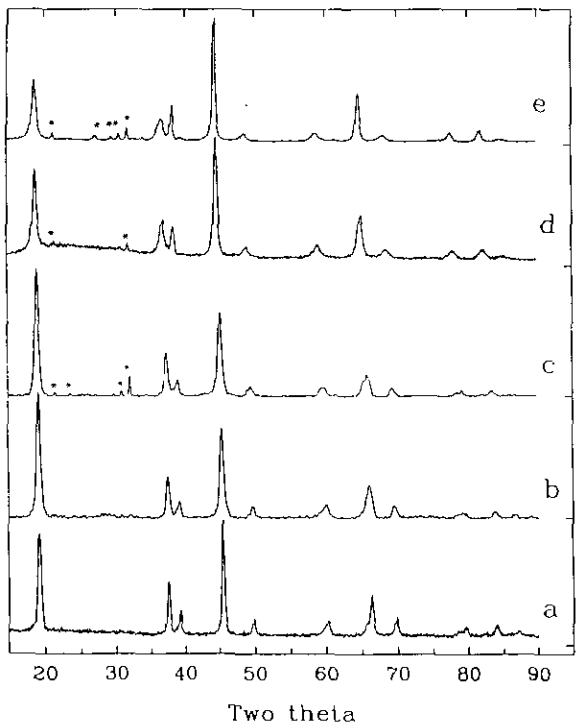

FIG. 1. XRD patterns of the products obtained by LT synthesis at 450°C. (*) Li_2CO_3, LiOH impurities. Ni/(Ni + Co): (a) 0.0, (b), 0.2 (c) 0.4, (d) 0.8, and (e) 0.9.

oxides, for which the XRD patterns are given in Fig. 1. These patterns can be indexed in the $R\bar{3}m$ space group (s.g.) as for other Li–Ni–O and Li–Co–O oxides prepared at high temperature and reported in the literature (11, 12). For Ni-rich LT samples, the synthesis procedure used in this study allows the preparation of layered oxides, although some impurities, basically lithium carbonate, are present in low contents (Fig. 1). It is important to note that, in contrast to LiOH, Li_2CO_3 does not interact with Ni-rich oxides.

The chemical composition and unit cell parameters of LT samples are shown in Table 1. For the sake of comparison, the same table contains the data on chemical composition and unit cell parameters for the layered $Li_{1-x}(Ni_yCo_{1-y})_{1+x}O_2$ oxides ($R\bar{3}$m s.g.) with the equivalent Ni/(Ni + Co) ratios and prepared at high temperature (850°C). As in the case of HT samples, the higher oxidation states of the transition metal atoms are found for Co-rich LT compositions. It is noteworthy that LT samples show a lower average oxidation state as compared to that of HT analogues. This can also be related with a lower c parameter, as well as with a lower c/a ratio representing the trigonal distortion of the cubic lattice. The a parameters of LT and HT samples are similar and increase as Ni amount increases, thus indicating the formation of the solid lithium–nickel–cobalt solution at low and high temperature. The above results allow to describe the LT and HT compositions with one and the same model: $Li_{1-x}M_{1+x}O_2$.

The possibility that LT mixed oxides had a spinel-related structure was examined by IR and Rietveld refinement procedures. Figure 2 shows the IR spectra of selected LT compositions in the 400–800 cm^{-1} region, where Ni/CoO_6 vibrations are only resolved (13, 14). The presence of four IR bands in the spectra of LT samples is consistent with a coordination of the transition metal ions which departs from the regular octahedron. A trigonally distorted octahedron could describe more accurately these data. This coordination agrees with the rhombohedral model in which z_{oxygen} is different from 0.25. Furthermore, the Rietveld refinement was carried out in selected patterns and a good fit was observed by using $R\bar{3}m$ instead

TABLE 1

Composition and Unit Cell Parameters of Pristine and Chemically Delithiated Samples

	Ni/(Ni + Co)	Li/(Ni + Co)	Average OS	a (Å)	c (Å)	c/a	H_2O (wt%)
Initial LT	0.2	0.93[a]	2.93	2.823	13.94	4.939	—
	0.4	0.90[a]	2.90	2.838	14.00	4.935	—
	0.8	0.72[a]	2.72	2.850	14.09	4.944	—
Initial HT	0.2	0.96	2.96	2.825	14.03	4.965	—
	0.4	0.92	2.92	2.837	14.08	4.962	—
	0.8	0.85	2.85	2.867	14.11	4.920	—
Acid-treated LT	0.2	0.25	3.46	2.819	14.25	5.055	8.71
	0.4	0.18	3.47	2.823	14.11	5.000	4.54
	0.8	0.18	3.17	2.836	14.08	4.963	2.02
Acid-treated HT	0.2	0.33	3.60	2.807	14.40	5.131	—
	0.4	0.15	3.68	2.817	14.30	5.076	—
	0.8	0.24	3.67	2.817	14.33	5.089	—

[a] Values derived from the average oxidation state of Ni + Co.

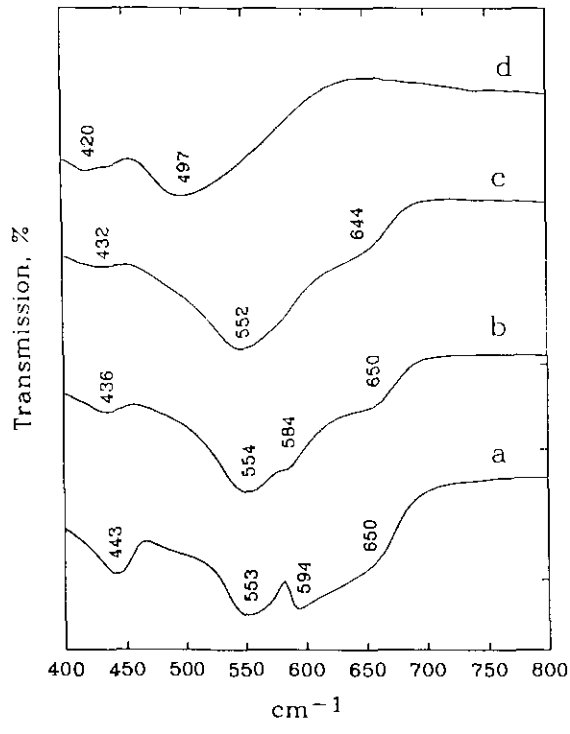

FIG. 2. IR spectra of the products obtained by LT synthesis. Ni/(Ni + Co): (a) 0.0, (b) 0.2, (c) 0.4, and (d) 0.8.

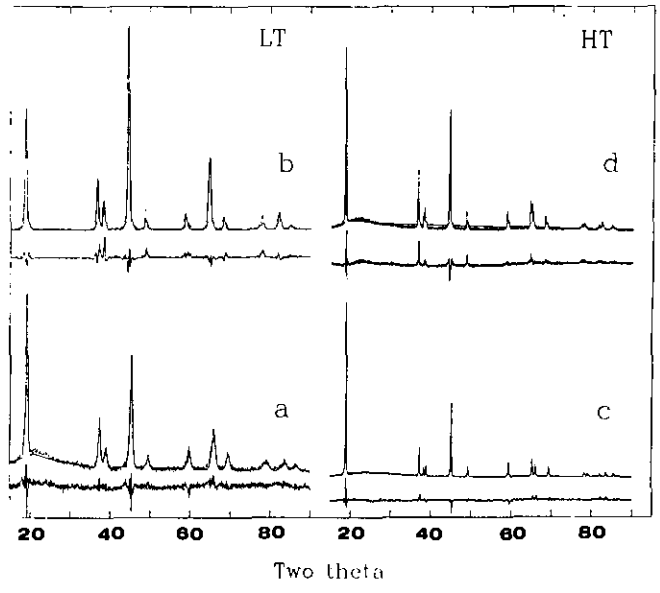

FIG. 3. Experimental, calculated and difference profiles obtained by Rietveld analysis in $R\bar{3}m$ s.g. Ni/(Ni + Co): (a, c) 0.2; (b, d) 0.8.

of $Fd3m$ s.g., as shown in Fig. 3. In addition, the IR spectra and X-ray diffraction data show a more pronounced cation disorder in the LiO_2 and MO_2 layers and a less marked trigonal distortion for high Ni/(Ni + Co) ratios in LT samples.

In conclusion, monophase $Li_{1-x}(Ni_yCo_{1-y})_{1+x}O_2$ oxides with the layered structure have been synthesized for the $0 \leq y \leq 0.4$ and $0.8 \leq y \leq 0.9$ ranges at low temperature (450°C). As in the case of HT samples, cobalt substitution for nickel favors the stabilization of Ni^{3+} ions and improves the two-dimensionality of the crystal structure.

Chemical Deintercalation Reactions

The effect of HCl treatment on the composition of the mixed oxides was followed by determining the amount of metal ions dissolved as a function of time. Figure 4 shows a plot of these results for selected compositions. As the Ni/Co ratio remained unchanged with acid treatment, as determined by AAS in the solution and by EDX in the solid products, Fig. 4 includes the changes in total transition metal content M and lithium. For both initial compositions the degree of deintercalation (M/Li) increases gradually with time. Although for low reaction periods, the degree of dissolution increases more abruptly for Co-rich compositions, it stabilizes to a lower value than Ni-rich samples after 300 min. The final compositions of the acid treated solids are included in Table 1. Complete extraction of lithium could not be achieved. However, the resulting contents make these materials interesting candidates for lithium insertion processes.

The XRD patterns (Fig. 5) and IR spectra (Fig. 6) of HT and LT chemically delithiated samples show that the layered rhombohedral structure is preserved during acid

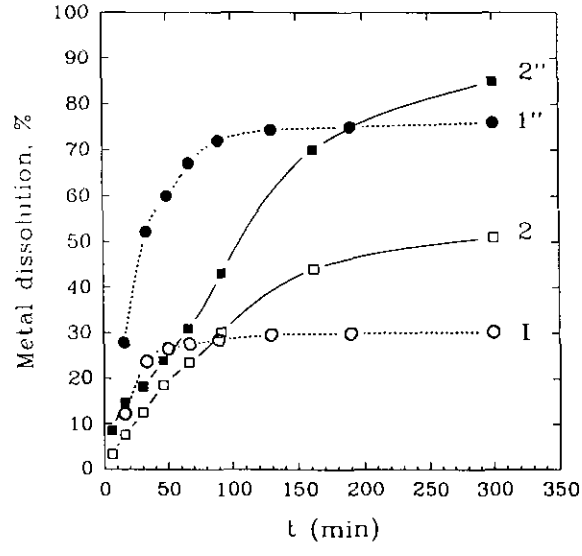

FIG. 4. Degree of metal dissolution vs time plots of selected HT samples. Ni/(Ni + Co) = 0.2, (Ni + Co) (1), Li (1''); Ni/(Ni + Co) = 0.8, (Ni + Co) (2), Li (2'').

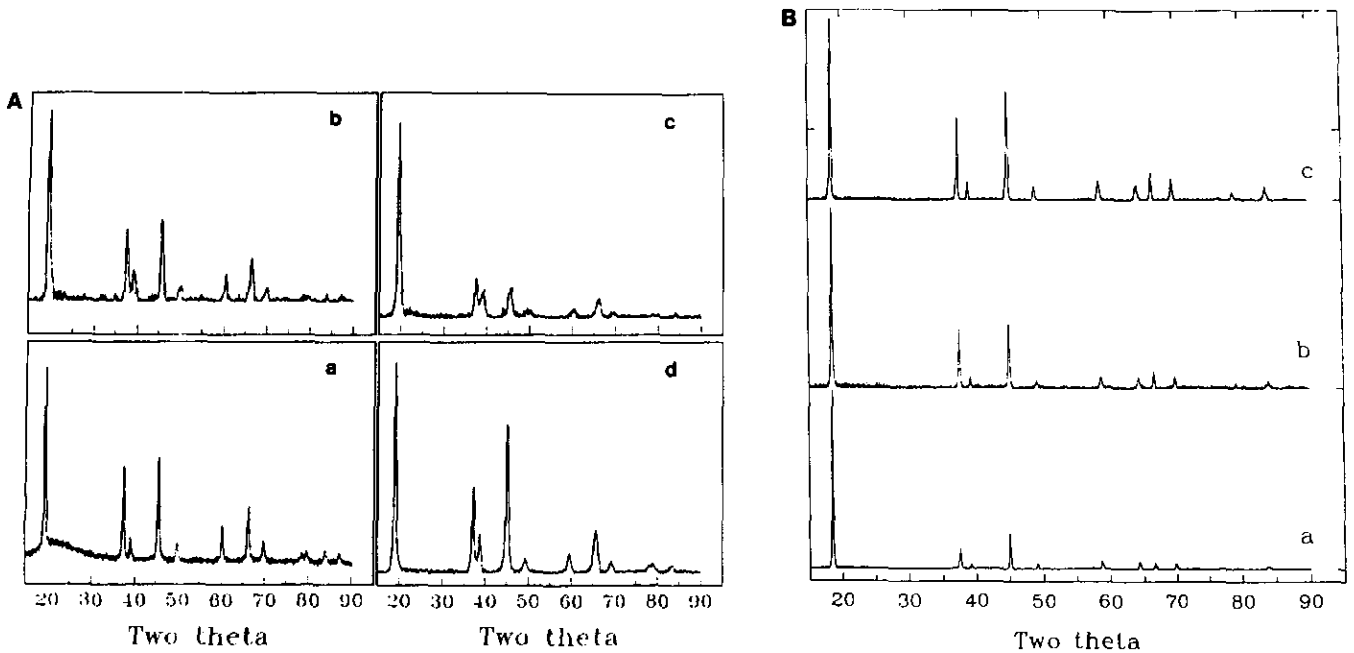

FIG. 5. (A) XRD patterns of chemically delithiated products. (A) LT samples, Ni/(Ni + Co): (a) 0.0, (b) 0.2, (c) 0.4, and (d) 0.8. (B) HT samples, Ni/(Ni + Co): (a) 0.2, (b), 0.4, and (c) 0.8.

treatment. A significant increase in average oxidation state of transition metal ions, c parameter, c/a ratio is observed in the deintercalated products of all compositions (Table 1) on account of the decreased lithium content in the interlayer space. Irrespective of the sample-preparation temperature, the more pronounced expansion of the c-axis is established for Co-rich compositions. This phenomenon is in agreement with the electrochemically

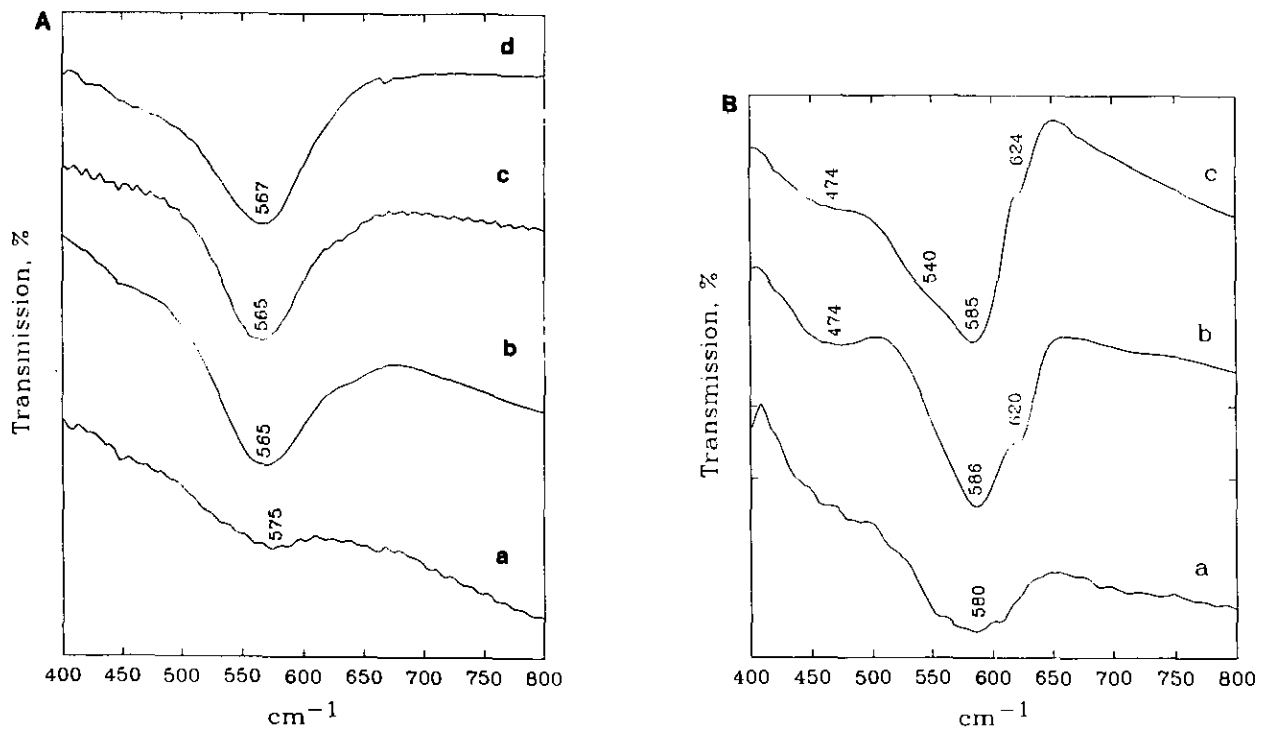

FIG. 6. (A) IR spectra of chemically delithiated products. (A) LT samples, Ni/(Ni + Co): (a) 0.0, (b) 0.2, (c) 0.4, and (d) 0.8. (B) HT samples, Ni/(Ni + Co): (a) 0.2, (b), 0.4, and (c) 0.8.

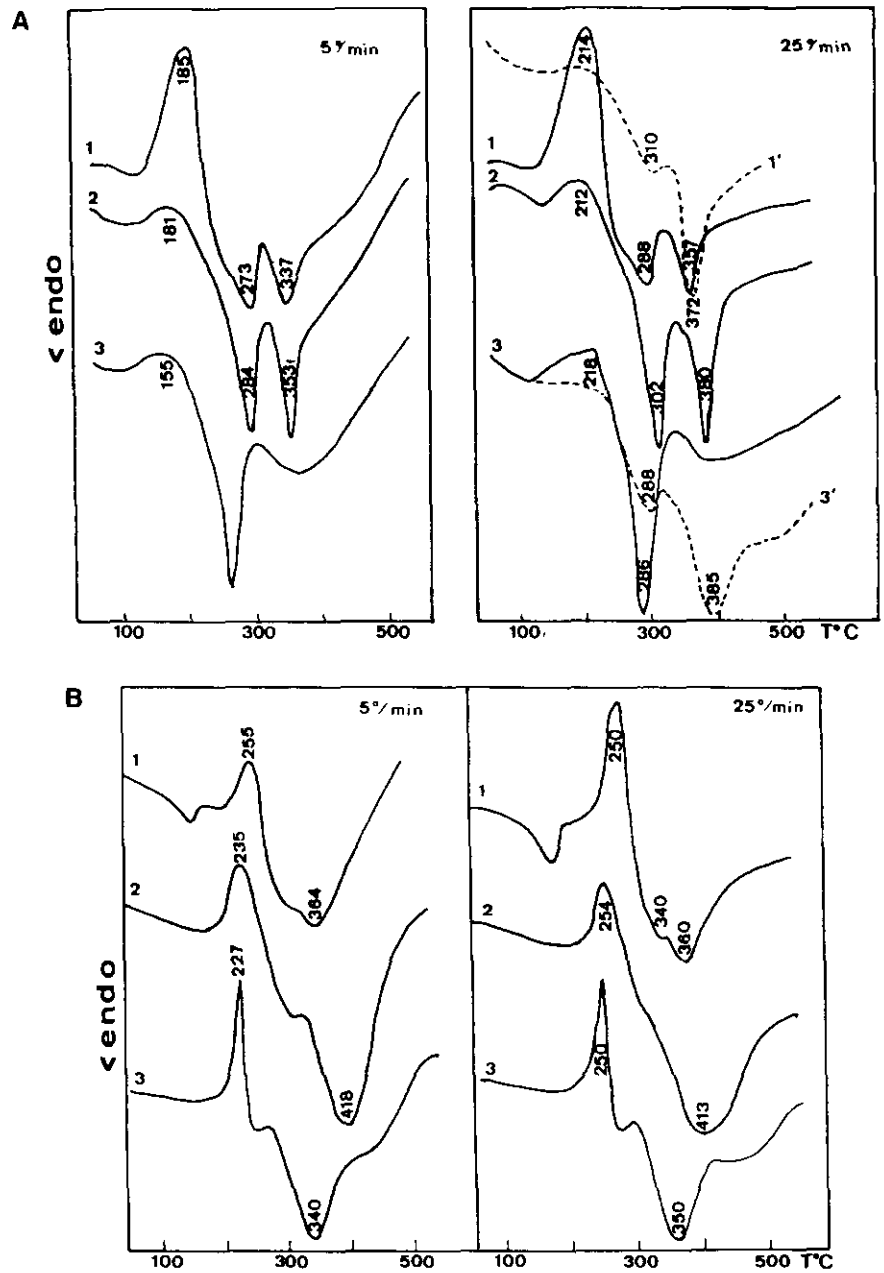

FIG. 7. DSC traces under static air atmosphere of chemically delithiated products (A) LT samples, Ni/(Ni + Co): (1) 0.2, (2) 0.4, and (3) 0.8, denotes diluted acid treatments. (B) HT samples, Ni/(Ni + Co): (1) 0.2, (2), 0.4, and (3) 0.8.

delithiated HT Li_xCoO_2, when the c-axis increases significantly between $0.75 \leq x \leq 0.93$ (5). Moreover, the oxidation of Ni and Co during acid extraction of Li is also manifested by the strong contraction in the a-axis, which has a weaker dependence on Ni/(Ni + Co) ratio in comparison with that for initial $Li_{1-x}(Ni_yCo_{1-y})_{1+x}O_2$ oxides. This result may explain the common features of the IR spectra of the acid-treated samples with a different Ni amount, if we consider the relationship between the normal vibration frequency and the distance of vibrating particles (well known "$r^{-3/2}$" law). The increase in average oxidation state of metal ions with acid treatment is more marked for Ni-rich HT samples. It is worth noting that acid-treated LT samples have a lower M average oxidation state and Li/M ratios. This means that the stoichiometry of the products must include either transition metal ions in the interlayer space or protons partially substituting for lithium ions at the interlayer space. In fact, Li/H

exchange has been reported for $LiCoO_2$ and $LiNi_xCo_{1-x}O_2$ (15). In addition, the presence of occluded water resulting from the acid treatment cannot be discarded.

In order to evaluate the thermal stability of the deintercalated products and the possible occurrence of partial H^+/Li^+ ion exchange during acid treatment, DSC, TG, and mass spectrometry of the gaseous products were performed. As shown recently (3, 4, 16), chemically delithiated $LiCoO_2$ and $Li_{1-x}Ni_{1+x}O_2$ display complex thermal behavior: on heating, cation redistribution is initiated in the layered structural framework of the metastable phase, culminating above 230°C in thermal transformation into a lithium–cobalt (or nickel) spinel. Figures 7 and 8 show the DSC and TG curve of acid delithiated LT and HT $Li_{1-x}(Ni_yCo_{1-y})_{1+x}O_2$. These curves consist of an exothermal effect located in the 220–260°C interval for HT samples and between 150 and 220°C for LT samples, which reflects the cation redistribution in octahedral (3*a* and 3*b*) and distorted tetrahedral sites of the trigonal framework, leading to the spinel-related phase. On further heating, endothermal effects take place: for LT oxides, there are two well resolved endotherms, while for HT oxides, a broad peak is spread between 230 and 450°C. These effects are accompanied by water and oxygen release, according to mass spectrometry measurements and the TG data in Fig. 8. While for HT Ni-rich samples, the weight loss can be almost completely ascribed to oxygen resulting from the reduction of nickel and formation of rock-salt type (15) phase, LT Co-rich samples contain significant amounts of hydrogen which is released as water at 300°C. This effect was evident by recording the DSC traces in samples treated with different concentrations of hydrochloric acid (Fig. 7A). The intensity of the 280–300°C endotherm decreases with acid concentration, which allows one to ascribe this process to water release. From TG curves of LT and HT samples, we can estimate the total amount of the released water (Table 1), but we are not able to determine the exact amount of the ion exchanged protons and the occluded water. Summarizing, thermal properties of acid treated LT and HT oxide reveal that the presence of cobalt and the low preparation temperature favors Li^+/H^+ ion exchange during acid treatment (endotherm peak at 280–300°C).

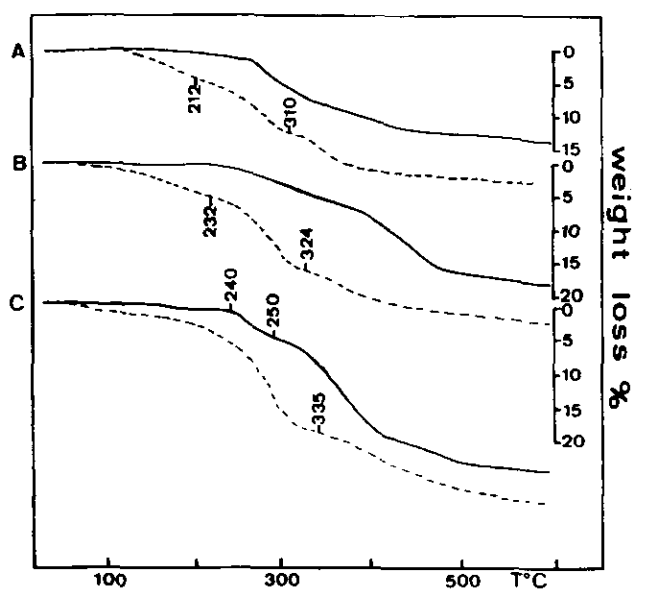

FIG. 8. TG traces of HT (—) and LT (---) acid treated samples with Ni/(Ni + Co): (A) 0.2, (B) 0.4, and (C) 0.8.

Further evidence of the ease of transformation of the chemically deintercalated solids to spinel-related structures was obtained by direct observation of the changes induced by electron radiation in the transmission electron microscope. The layered habit of LT samples is exemplified in Fig. 9a in which lattice fringes are observed in particles oriented perpendicularly to [001]. During observation of the acid treated samples at low electron-accelerating voltage (120 kV) most particles exhibit smooth surface and an electron diffraction pattern which can be considered a result of the coexistence of three domains with orientations differing from each other by 60°. Each domain is near the [110], zone and the superimposition of the three arrays of spots leads to an hexagonal distribution as that shown in Fig. 9b and lattice fringes in Fig. 9c. This pattern is not observed in the pristine solid and can be considered a result of the changes induced by chemical extraction of lithium by opening pathways for ion transport. When higher voltages (200 kV) and electron beam intensities were used, a transformation of the particles could be observed that conditions the occurrence of a complex texture of the solid (Fig. 9c). In addition, $[11\bar{1}]$ and $[1\bar{1}1]$ lattice fringes forming 109.5° angles are observed (Fig. 9d), which are consistent with the [110] zone of an $Fd\bar{3}m$ phase.

Electrochemical Behavior of Deintercalated Samples

Selected chemically deintercalated samples were used as cathode material in lithium cells. As the average oxidation state of metal ions were in the 3+–4+ interval and Li/*M* ratios were between 0.2 and 0.4, the resulting cells showed high values of initial voltage (about 4 V) that allow the direct discharge of the cells without previous charge.

Typical voltage vs composition results of the step potential electrochemical spectroscopy of lithium cells are shown in Fig. 10 for HT samples. For both compositions, the discharge of the cells allow final Li contents (Li/*M* = 0.90 and 0.74) close to those found for the initial HT samples (Li/*M* = 0.96 and 0.85; see Table 1), the difference being more prominent for Co-rich samples, probably as a consequence of the partial Li^+/H^+ exchange found

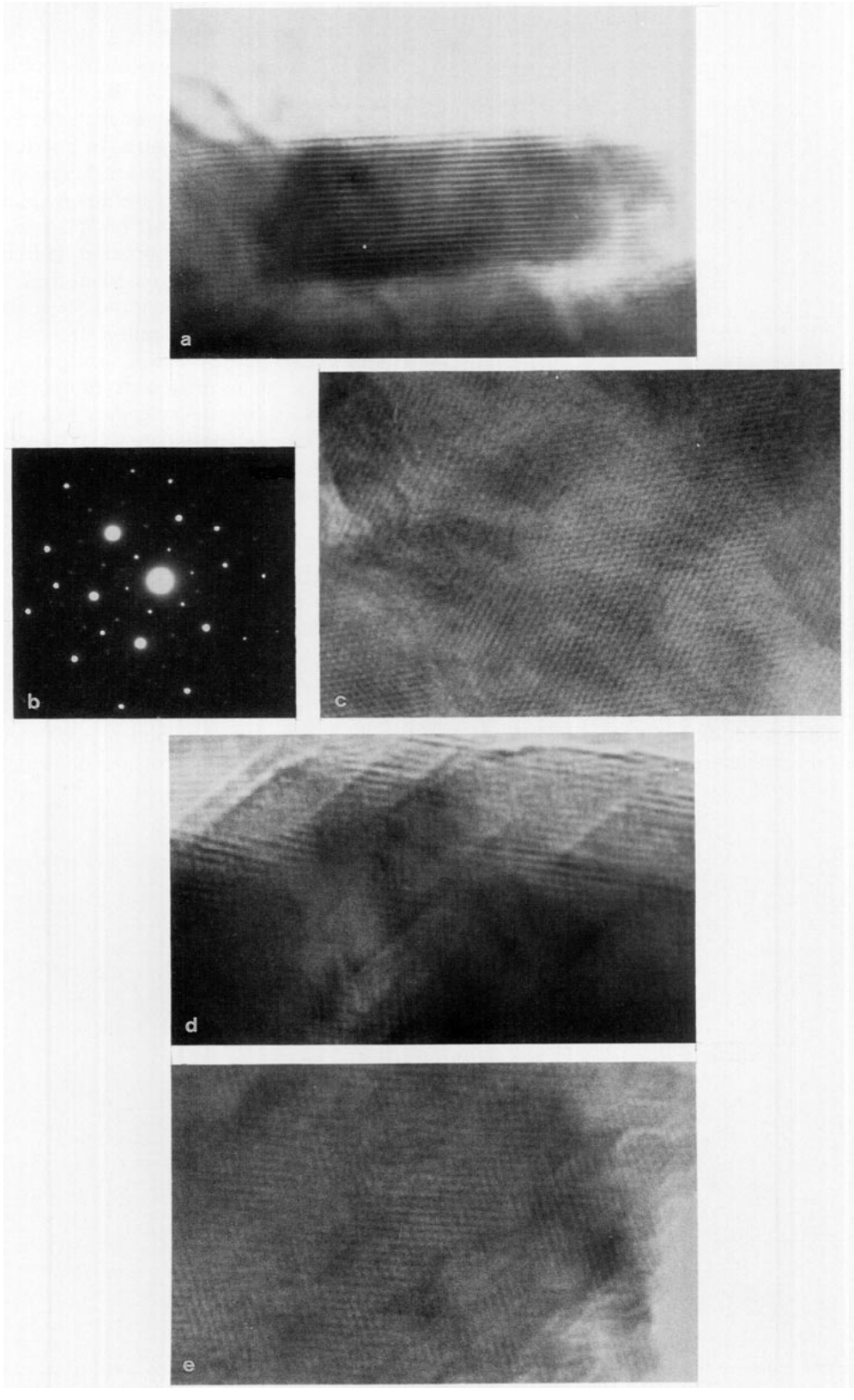

FIG. 9. Electron micrographs of (a) pristine LT-Ni/(Ni + Co) = 0.2 showing (001) fringes. (b) Three orientation [110] zone electron diffraction pattern of acid-treated HT-Ni/(Ni + Co) = 0.8, (c) lattice fringes forming domains separated by 60° in acid-treated LT-Ni/(Ni + Co) = 0.8, (d) lattice fringes of acid-treated HT sample Ni/(Ni + Co) = 0.2 transformed *in situ* to spinel oxides, and (e) lattice fringes forming 109° of transformed acid-treated LT sample Ni/(Ni + Co) = 0.8.

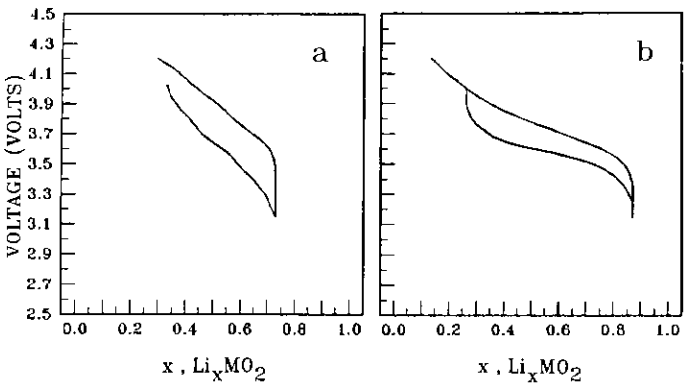

FIG. 10. Voltage vs composition curves obtained by step potential electrochemical spectroscopy of acid-treated HT samples with Ni/(Ni + Co) = 0.2 (a) and 0.8 (b).

for Co-rich compositions. Charging the cell again results in a better reversibility for Ni-rich oxide. However, the composition of the acid treated solid can be recovered without an enhanced polarization of the cells.

XRD patterns and IR spectra of the cathode Ni-rich material after cell discharge and charge are compared with those of pristine and acid-treated samples in Fig. 11. These data show remarkable similarities which can be interpreted in terms of a good reversibility of lithium insertion–extraction by chemical and electrochemical procedures.

For LT samples, the final charge composition (Fig. 12) has a larger departure from the chemical composition of pristine oxides, as a result of the larger amount of hydrogen present in the structure. In addition, the discharge and charge processes occur at lower voltage (especially for Co-rich samples) and the reversibility of the cells is lower as compared to that of HT analogues. While for LT Ni-rich oxides the discharge and charge curves are typical for a single-phase reaction, for LT Co-rich oxides, curves with plateaus at 3.52–3.49 V for discharge and 3.55–3.68 V for charge reflect the two-phase reaction. The same two-phase reaction was founded for LT-$LiCoO_2$ (7, 8) with a spinel-related structure. The plateaus in the charge and discharge curves were explained by the coexistence between spinel-related LT-$LiCoO_2$ and spinel-related $Li_{0.5}CoO_2$ (7, 8). Due to the similarity between XRD patterns of the layered ($R\bar{3}m$ s.g.) and spinel ($Fd3m$) structures (8), IR spectroscopy is used (Fig. 13) to follow the changes in $Ni_{0.2}Co_{0.8}O_2$ layers after discharge of the LT Co-rich oxide to 3 V. The recovery of the initial IR spectrum, when oxide reacts only with 0.3 equivalents of lithium (Fig. 12a), implies that the two-phase reaction in discharge–charge curves is most probably a result of the coexistence of the layered phases ($LiMO_2$ and $Li_{1-x}MO_2$) with a different degree of trigonal distortion. Unfortunately, we are not able, on basis of this data, to estimate the degree of trigonal distortion of MO_6-octahedron,

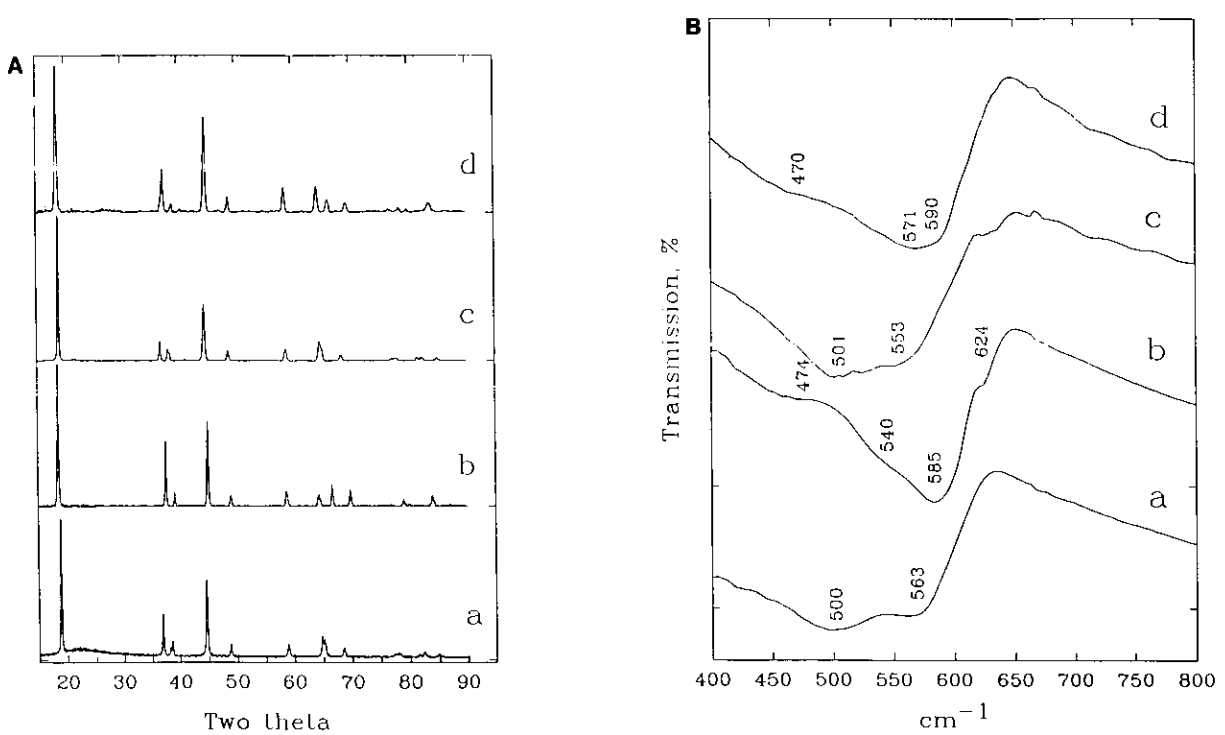

FIG. 11. XRD patterns (A) and IR spectra (B) for HT-Ni/(Ni + Co) = 0.8 (a) initial sample, (b) acid-treated sample, (c) after discharge of the cell to 3 V, and (d) after charge of the cell to 4 V.

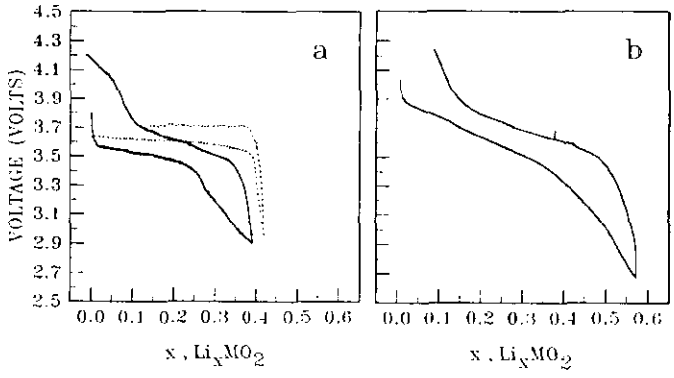

FIG. 12. Voltage vs composition curves obtained by step potential electrochemical spectroscopy of acid-treated LT samples with Ni/(Ni + Co) = 0.2 (a) and 0.8 (b). For comparison, discharge and charge curves of $LiCoO_2$, obtained from $Co(OH)_2$ and LiOH at 450°C, are also shown.

which may throw new light on the lower charge and discharge voltages of LT electrodes as compared to that of HT analogues.

On the other hand, the voltages found at the initial steps of the discharge are higher for the Co-rich composition, as expected for the higher potential of Co^{4+}/Co^{3+} as compared with Ni^{4+}/Ni^{3+}. A plot of the incremental capacity vs voltage of the HT samples (Fig. 14) shows a single peak for Ni-rich composition located at 3.58 V during discharge and 3.64 V during charge. According to previous studies on $Li_{1-x}NiO_2$, this peak can be unambiguously ascribed to Ni^{4+}/Ni^{3+} reduction. For the Co-rich HT sample, the pattern is more diffuse but new peaks at 3.84 V (discharge) and 3.92 V (charge) occur which may be related to cobalt reduction.

CONCLUSIONS

The main conclusions that can be derived from the above results are summarized as follows:

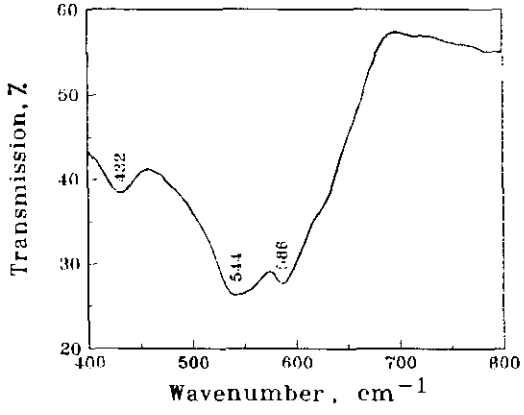

FIG. 13. IR spectrum for LT-Ni/(Ni + Co) = 0.2 after discharge of the cell to 3V.

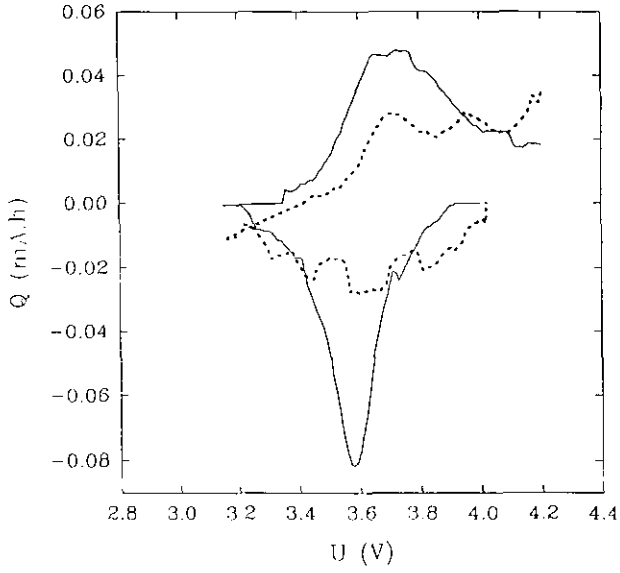

FIG. 14. Incremental capacity vs voltage curves for discharge–charge of cells using acid-treated HT samples with Ni/(Ni + Co) = 0.8 (—) and 0.2 (---).

—It is possible to prepare lithium–nickel–cobalt oxides with layered structures in the $0 \leq y \leq 0.4$ and $0.8 \leq y \leq 0.9$ composition interval at different temperatures. Higher lithium contents and average oxidation states of transition metals are obtained for HT synthesis and for Co-rich compositions.

—Acid treatment of both sets of samples leads to a partial dissolution of the solid and the occurrence of a chemically deintercalated solid in which the rhombohedral layered structure is preserved and the average oxidation state of metal ions increases significantly. For Co-rich samples, the process is accompanied by partial Li/H exchange, specially in LT samples.

—The chemically deintercalated materials have a low thermal stability, and cation redistribution is easily accomplished leading to spinel-related structures.

—The electrochemical insertion of lithium into acid-treated materials can be carried out during the discharge of lithium cells. The resulting products recover the lithium content and structural characteristics of the unreacted solid. A good reversibility of the cells is particularly found for HT Ni-rich oxides in the 4.0–3.2 V range.

ACKNOWLEDGMENT

The authors thank the Commission of the European Communities for financial support in the form of a research fellowship ("Go West") to the program "Cooperation in Science and Technology with Central and Eastern European Countries" (Contract CIPA-CI-92-0131) and a contract (JOU2-CT93-0326) of the Joule II program.

REFERENCES

1. T. Nagaura and K. Tazawa, *Prog. Batteries Sol. Cells* **9,** 20 (1990).
2. J. R. Dahn, U. Von Sacken, M. R. Jukow, and H. Al-Janaby, *J. Elelectrochem. Soc.* **137,** 2207 (1991).
3. J. Morales, C. Perez-Vicente, and J. L. Tirado, *Mater. Res. Bull.* **25,** 623 (1990).
4. R. Stoyanova and E. Zhecheva, *J. Solid State Chem.*, in press.
5. J. N. Reimers and J. R. Dahn, *J. Electrochem. Soc.* **139,** 2091 (1992).
6. C. Delmas and I. Saadoune, *Solid State Ionics* **53–56,** 370 (1992).
7. R. J. Gummow, D. C. Liles, and M. M. Thackeray, *Mater. Res. Bull.* **28,** 235 (1993).
8. E. Rossen, J. N. Reimers, and J. R. Dahn, *Solid State Ionics* **62,** 53 (1993).
9. R. J. Gummow and M. M. Thackeray, *Solid State Ionics* **53–56,** 681 (1992).
10. D. B. Wiles and R. A. Young, *J. Appl. Crystallogr.* **14,** 149 (1981).
11. J. B. Goodenough, D. G. Wickman, and W. J. Croft, *J. Phys. Chem. Solids* **5,** 107 (1958).
12. H. J. Orman and P. J. Wiseman, *Acta Crystallogr. Sect. C.* **40,** 12 (1984).
13. R. K. Moore and W. B. White, *J. Am. Ceram. Soc.* **53,** 679 (1970).
14. P. Tarte and J. Preudhomme, *Spectrochim. Acta* **26A,** 747 (1970).
15. E. Zhecheva and R. Stoyanova, *J. Solid State Chem.*, in press.
16. J. Morales, C. Perez-Vicente, and J. L. Tirado, *J. Thermal Anal.* **38,** 295 (1992).